Evidence for enhancement of vortex matching field above 5 T and oxygen-deficient annuli around barium-niobate nanorods

Shigeru Horii, Masakazu Haruta, Ataru Ichinose, and Toshiya Doi

---

Articles you may be interested in

Strongly enhanced vortex pinning from 4 to 77 K in magnetic fields up to 31 T in 15 mol.% Zr-added (Gd, Y)-Ba-Cu-O superconducting tapes
APL Mat. **2**, 046111 (2014); 10.1063/1.4872060

Anisotropy and directional pinning in YBa2Cu3O7− x with BaZrO3 nanorods
Appl. Phys. Lett. **103**, 022603 (2013); 10.1063/1.4813405

The effects of strain, current, and magnetic field on superconductivity in Pr0.5Ca0.5MnO3/YBa2Cu3O7/Pr0.5Ca0.5MnO3 trilayer
J. Appl. Phys. **113**, 113902 (2013); 10.1063/1.4795349

Flux pinning properties and microstructure of SmBa 2 Cu 3 O y thin films with systematically controlled BaZrO 3 nanorods
J. Appl. Phys. **108**, 093905 (2010); 10.1063/1.3498812

Flux pinning properties in BaMO 3 (M = Zr , Sn) nanorod-introduced ErBa 2 Cu 3 O x films
J. Appl. Phys. **106**, 103915 (2009); 10.1063/1.3257260

Evidence for enhancement of vortex matching field above 5 T and oxygen-deficient annuli around barium-niobate nanorods

Shigeru Horii,[1,a)] Masakazu Haruta,[2] Ataru Ichinose,[3] and Toshiya Doi[1]

[1]*Graduate School of Energy Science, Kyoto University, Yoshida-Honmachi, Sakyo-ku, Kyoto, Kyoto 606-8501, Japan*
[2]*Doshisha University, Kyotanabe, Kyoto 610-0321, Japan*
[3]*Central Research Institute of Electric Power Industry, Yokosuka, Kanagawa 240-0196, Japan*

We report the dependence of critical temperature (T_c), the irreversibility line, the microstructure of nanorods with perovskite-based barium niobates (BNOs), and the c-axis length of the YBa$_2$Cu$_3$O$_y$ (Y123) superconducting matrix on the BNO-doping level and growth temperature for Y123 thin films with BNO nanorods. The characteristic field (B_{cr}) determined from the vortex-Bose-glass-like irreversibility lines in Y123+BNO films is strongly correlated to the BNO nanorod density and the growth temperature. Despite a monotonic decrease in T_c with increasing B_{cr} and nanorod density, the irreversibility fields (B_{irr}) were enhanced up to $B_{cr} \sim 5$ T. From the B_{cr} value and the mean diameter of the BNO nanorod (~ 10 nm), we estimate that a lower T_c matrix annulus with a diameter of 12–14 nm exists around each BNO nanorod due to the strong interface strains. Our present study suggests that generation of this lower T_c region around each BNO nanorod increases the vortex-pinning strength significantly and, moreover, may offer a new way of enhancing B_{irr} for REBa$_2$Cu$_3$O$_y$ film with nanorods. © *2015 AIP Publishing LLC.*
[http://dx.doi.org/10.1063/1.4932529]

INTRODUCTION

Further improvement of critical current properties in second-generation REBa$_2$Cu$_3$O$_y$ (RE123; RE: rare earth elements)-coated conductors is a serious issue for magnet applications. The introduction of defects or a non-superconducting rod-shaped secondary phase into RE123 matrix films is an effective process for increasing the irreversibility field (B_{irr}) and enhancing the in-field critical current density (J_c) in a magnetic field (B) parallel to the c-axis. Especially in biaxially oriented RE123 films prepared by pulsed laser deposition (PLD), nanorods as the non-superconducting secondary phase can be introduced easily by using bulk RE123 targets containing an appropriate nanorod material as one-dimensional vortex-pinning centers. Since this simple but practically important technique for the introduction of rod-shaped vortex-pinning centers was developed by MacManus-Driscoll et al.,[1] a large number of leading-edge researches and developments have been performed to improve superconducting properties under magnetic fields in RE123 films with nanorods. For example, the maximization of J_c (Ref. 2) and vortex-pinning force density[3] by controlling the nanorod-doping level,[4] the introduction of nanorods without T_c reduction,[2] the understanding of vortex-pinning states around B_{irr},[5,6] and the equalization of the magnetic-field-angle dependence of J_c[7,8] have been reported. Furthermore, various nanorod materials, such as BaZrO$_3$ (BZO),[1,9–14] Ba-Nb-O (BNO),[5,6,15–18] Ba-Ta-O,[19] Ba-W-O,[20] Ba-Hf-O,[21] and BaSnO$_3$,[3] have been reported at the current stage, and it is recognized that perovskite-based barium oxides are preferable dopants for the formation of

nanorods. In addition to the above reports, optimization of the microstructures of both the RE123 matrix and nanorods has also been attempted for the improvement of superconducting properties under magnetic fields in RE123 films with nanorods. For example, it was reported that growth temperature was also a determining factor in the enhancement of the in-field J_c[12,13,17] and B_{irr},[6] which originated from growth-temperature-dependent microstructures and nanorod densities. Very recently, B_{irr} values over 14 T at 77.3 K (Refs. 22 and 23) have been successfully achieved in Gd-based 123 films with nanorods by controlling the crystallinity of the (Gd,Y)123 matrix to overcome the T_c reduction due to the nanorods[14] and morphology of Ba-Hf-O nanorods.[23]

One of the most interesting features on RE123 films with nanorods is the appearance of a vortex-Bose-glass-like irreversibility line (IL).[5] In the case of RE123 films with Ba-Nb-O-based nanorods, our group clarified that a boundary field (B_{cr}) between strong and weak Bose-glass states was sensitive to the growth (or substrate) temperature[6] and type of RE[24] in RE123. While studying heavy-ion-irradiated Y123 crystals, Krusin-Elbaum et al.[25] found that B_{cr} is strongly correlated with the density of the columnar defects introduced. The reports above indicate that the changes in B_{cr} that depend not only on the doping level of the nanorod material but also on the growth conditions and matrix compounds lead directly to a serious problem related to maximization of the vortex-pinning efficiency of nanorods for improvement of the in-field J_c from the viewpoint of practical applications. Recently, Cantoni et al.[26] reported that the strain-induced oxygen-deficient matrix region existed at a matrix/nanorod interface, and the distance of the region from the interface was approximately ~ 10 nm for a Y123 film

a)Author to whom correspondence should be addressed. E-mail: horii.shigeru.7e@kyoto-u.ac.jp.

with BZO nanorods. However, the relationship between vortex-pinning properties and microstructures with unstrained and strained regions in RE123 films that contain nanorods is not yet understood. In the present study, using Y123 thin films that contained BNO nanorods grown at various substrate temperatures by PLD using Y123 targets with different BNO-doping levels, their ILs, cross-sectional microstructures, and lattice parameters were clarified. Furthermore, these results provide an estimation of the distance from the interface to the Y123 matrix region with strain-induced lower T_c without precise spatial analyses[26] of the chemical composition, c-axis length, and valence of the Cu ion using an electron nanobeam.

EXPERIMENTAL

BNO-doped Y123 films with a thickness of 200–300 nm were grown on (100) SrTiO$_3$ (STO) substrates by PLD using bulk targets with a mixture of Y123 + x at. % BaNb$_2$O$_6$ ($x = 0$, 2.5, 5.0, and 7.5). Here, PLD was performed using a Q-switched Nd:YAG laser with its fourth harmonics operating at the wavelength of 266 nm; the repetition rates of the flash lamp and Q-switch were 10 and 2 Hz, respectively. Biaxially oriented films with $c\perp$ substrate surfaces were obtained in a substrate temperature (T_s) range from 850 to 890 °C under an oxygen pressure [$P(O_2)$] of 20 Pa. Incidentally, T_s values were determined using a thermocouple mounted on an SiC heater. *In situ* post-annealing was performed at 450 °C under $P(O_2) \sim 2 \times 10^4$ Pa for 1 h. T_c and B_{irr} of $\sim$100-μm-wide oxygen-annealed films were characterized by the four-probe method under various magnetic fields applied parallel to the c-axis and were determined by the temperature at which electrical resistivity (ρ) became $\rho/\rho(93\,\mathrm{K}) = 10^{-3}$ under each magnetic field with $B//c$. Cross-sectional microstructures were observed using transmission electron microscopy (TEM). Lattice parameters of the Y123 matrix and BNO nanorods were determined by reciprocal space mapping (RSM) measurements of the (108) and (018) planes for Y123 and the (206) plane for BNO with a double-perovskite crystal structure.[15,16]

RESULTS

T_c values for the BNO-free Y123 films and BNO-doped Y123 films ($x = 2.5$, 5.0, and 7.5 at. %) that were grown at various T_s conditions are listed in Table I. Most of the BNO-free Y123 films exhibited $T_c \sim 90$ K. Although the BNO-free films grown at $T_s = 870$ °C showed a T_c that was approximately 2 K lower, all BNO-free films were in an optimal

carrier-doping level. One can roughly see that T_cs were not largely affected by T_s. In the case of the BNO-doped films with $x = 2.5$ and 5.0 at. %, T_c slightly decreased with an increase in T_s, and difference in T_c (ΔT_c) between $T_s = 850$ and 890 °C was $\Delta T_c \sim 1$ K. However, in the BNO-doped Y123 films with $x = 7.5$ at. %, T_c remarkably increased with an increase in T_s, and the ΔT_c value was approximately 4 K.

Figures 1(a)–1(c) show irreversibility lines (ILs) for the BNO-doped Y123 films ($x = 2.5$, 5.0, and 7.5 at. %, respectively) grown at $T_s = 850$ to 890 °C. For reference, the IL for the BNO-free Y123 film grown at $T_s = 850$ °C is also shown. It should be noted that the reduced temperature (t), which is normalized by T_c, is represented as the abscissa axis in the figures. For example, the B_{irr} values at $t = 0.9$ were $\sim$4 T, 4.5–6 T, 7–10.5 T, and 9–12.5 T for the BNO-free film ($T_s = 850$ °C) with $x = 0$ at. %, 2.5 at. %, $x = 5.0$ at. %, and $x = 7.5$ at. %, respectively. Therefore, the B_{irr}s for all BNO-doped Y123 films in Fig. 1 were clearly shifted toward higher temperature and magnetic field regions by the BNO doping, and the effects of the expansion of the vortex-glass region became qualitatively larger with the increase in the nominal BNO-doping level. Furthermore, these characteristic ILs consisting of positive curvature and linear portions were vortex-Bose-glass-like[5,6,27] and can be understood in terms of a crossover from strong- to weak-vortex-Bose-glass states.[25,27–29]

Here, the crossover field (B_{cr}) was defined as the boundary field between the positive curvature and linear portions on each IL. In the strong-Bose-glass state below B_{cr}, all vortices are pinned strongly by the columnar defects, in principle, whereas there are also vortices pinned weakly by the interaction among vortices in the weak-vortex-Bose-glass state above B_{cr}. Therefore, the value of B_{cr} corresponds to the matching field (B_ϕ),[25,28] and the density of the nanorods introduced into the matrix can be estimated from the value of B_{cr}. The determined B_{cr} value for each IL is represented by an arrow in Fig. 1(b), and all of the determined B_{cr} values are summarized in Table II. It was found that B_{cr} systematically increased with an increase in T_s in the cases of $x = 2.5$ and 5.0 at. %. These T_s-dependent behaviors were quite a contrast to the result for $x = 7.5$ at. %. Although the origin of the different T_s dependence of B_{cr} has been unclear at the current stage, the present study found that the densities of the BNO nanorods were sensitive to T_s in addition to x.

Figures 2(a)–2(c) show cross-sectional TEM images of the BNO-doped Y123 films ($T_s = 890$ °C) with $x = 2.5$, 5.0, and 7.5 at. %, respectively. These cross-sectional images indicate that the morphologies of the BNO nanorods depended on the doping level of BNO. It was found as a qualitative tendency that long and linear nanorods were observed in the case of growth at a higher T_s, whereas the inter-nanorod distance was shortened or the nanorod density was increased with the increase in x. That is, cross-sectional TEM images for films grown at a lower T_s qualitatively suggested that short and bent nanorods were formed. To quantitatively clarify the details of the nanorod morphology for BNO-doped Y123 films, the diameter (d) and degrees of interruption and splay for the grown BNO nanorods were determined from cross-sectional TEM images. It should be

TABLE I. T_c values for BNO-doped Y123 films.

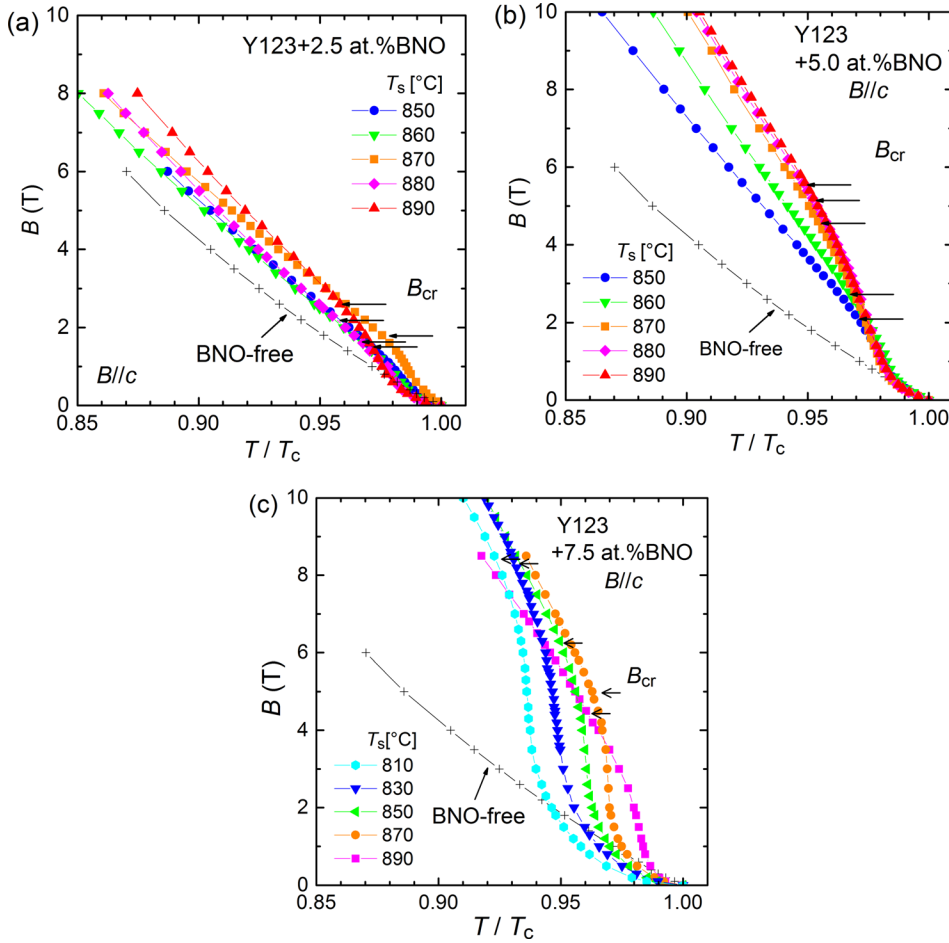|	T_c (K)				
x (at. %)	T_s (°C) = 850	860	870	880	890
0	90.69	89.54	88.29	91.08	90.35
2.5	88.14	-	87.59	-	87.07
5	84.77	-	84.12	-	83.56
7.5 (No. 1)	82.05	83.47	82.98	84.99	85.5
7.5 (No. 2)	80.1	-	81.45	-	84.82

FIG. 1. Irreversibility lines for BNO-doped Y123 films with $x =$ (a) 2.5, (b) 5, and (c) 7.5 at. %.

noted that the degrees of interruption and splay were evaluated as the averages of L_{rod}/L_{film} and $|\phi|$, where L_{rod}, L_{film}, and $|\phi|$ are length of the nanorods, thickness of the film, and angle between the c-axis of the matrix, and the elongated direction of the nanorods, respectively. T_s dependences of the mean L_{rod}/L_{film} and the $|\phi|$ values are shown in Figs. 3(a) and 3(b), respectively. As can be seen from Fig. 3(a), the values of L_{rod}/L_{film} increased with T_s in the BNO-doped Y123 films with $x = 2.5$ and 5 at. %; however, L_{rod}/L_{film} was close to 1, even with the change in T_s in $x = 7.5$ at. %. Furthermore, it is found from Fig. 3(b) that $|\phi|$ decreased with T_s in $x = 2.5$ and 5 at. % and was almost constant in $x = 7.5$ at. %. These results in Figs. 3(a) and 3(b) indicate that the nanorod morphology for the BNO-doped Y123 films is clearly sensitive to T_s and x. Figure 3(c) shows the T_s dependence of the mean d values for BNO-doped Y123 films. The d value tends to increase slightly with a decrease in T_s in the case of $x = 2.5$ and 5 at. %, whereas d slightly increased

with T_s for $x = 7.5$ at. %. Consequently, the d values were roughly estimated to be 10 nm for the BNO-doped Y123 films grown at $850\,^{\circ}\mathrm{C} \le T_s \le 890\,^{\circ}\mathrm{C}$.

To confirm generation of the lattice strain in the Y123 matrix by the doping of BNO nanorods for the BNO-doped Y123 films, the c-axis lengths of the matrix for the BNO-doped Y123 films were determined precisely from RSM measurements. Figures 4(a) and 4(b) show the RSM measurements of the BNO-free Y123 film ($T_s = 890\,^{\circ}\mathrm{C}$) and the BNO-doped Y123 film ($x = 5$ at. %, $T_s = 890\,^{\circ}\mathrm{C}$) as examples of Y123 films without and with BNO nanorods, respectively. Here, Q_x and Q_z are numbers in reciprocal space parallel to [100], ([010]), and [001]. In the case of the BNO-free film, clear split spots, which were identified as $(10l)$ and $(01l)$ [$l = 8$ and 9], were observed at $Q_x \sim 0.26\,\text{Å}^{-1}$ in addition to the spot due to (103) of the STO substrate. This is due to the coexistence of the a- and b-axes of the Y123 film, which is induced by twin microstructures parallel to the surface of the STO substrate. On the other hand, these split spots at the $(10l)$ and $(01l)$ planes disappeared for the BNO-doped Y123 film. This suggests a broadening of each diffraction spot in the Y123 matrix, which is induced by the introduction of the BNO nanorods. Incidentally, a diffraction spot due to the (206) plane of the BNO nanorods with a double-perovskite structure[15,16] was observed at $(Q_x, Q_z) = (\sim 0.24\,\text{Å}^{-1}, \sim 0.75\,\text{Å}^{-1})$; this spot was quite broadened.

Based on the above RSM measurements, a change in the c-axis length was clarified on the Y123 matrix for confirming

TABLE II. B_{cr} values for BNO-doped Y123 films.

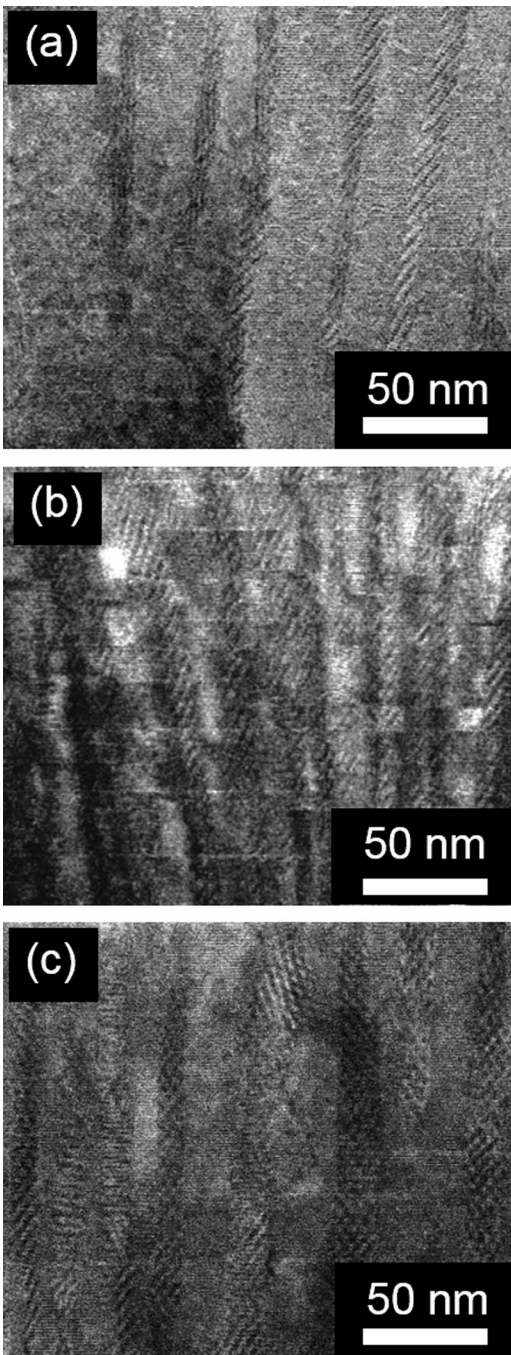|	B_{cr} (T)				
x (at. %)	$T_s\,[^{\circ}\mathrm{C}] = 850$	860	870	880	890
2.5	1.67	1.64	2.19	2.14	2.65
5	1.75	2.8	4.58	5.1	5.3
7.5 (No. 1)	5.95	5.36	5.07	3.54	3.3
7.5 (No. 2)	6.3	-	5.35	-	3.72

FIG. 2. Cross-sectional TEM images for BNO-doped Y123 films ($T_s = 890\,^\circ$C) with $x =$ (a) 2.5, (b) 5.0, and (c) 7.5 at. %.

FIG. 3. Changes in mean values of (a) L_{rod}/L_{film}, (b) ϕ, and (c) d of the BNO nanorods for BNO-doped Y123 films with $T_s = 850$, 870, and 890 °C as a function of T_s.

generation of the lattice strain in the Y123 matrix along the c-axis direction for the BNO-doped Y123 films. Figure 4(c) shows the relationship between c of the Y123 matrix and T_s for the BNO-free and BNO-doped ($x = 5$ at. %) films with $T_s = 850$, 870, and 890 °C, together with the c values for fully oxidized and reduced Y123 films on STO[30] for reference. The c-axis lengths of the obtained BNO-free films coincided well with that of the fully oxidized Y123 film, suggesting that the samples obtained in the present study were also oxidized. Moreover, the c-axis lengths of Y123 for the BNO-doped films were clearly larger than those for the BNO-free films in an entire T_s region, and the change in T_s
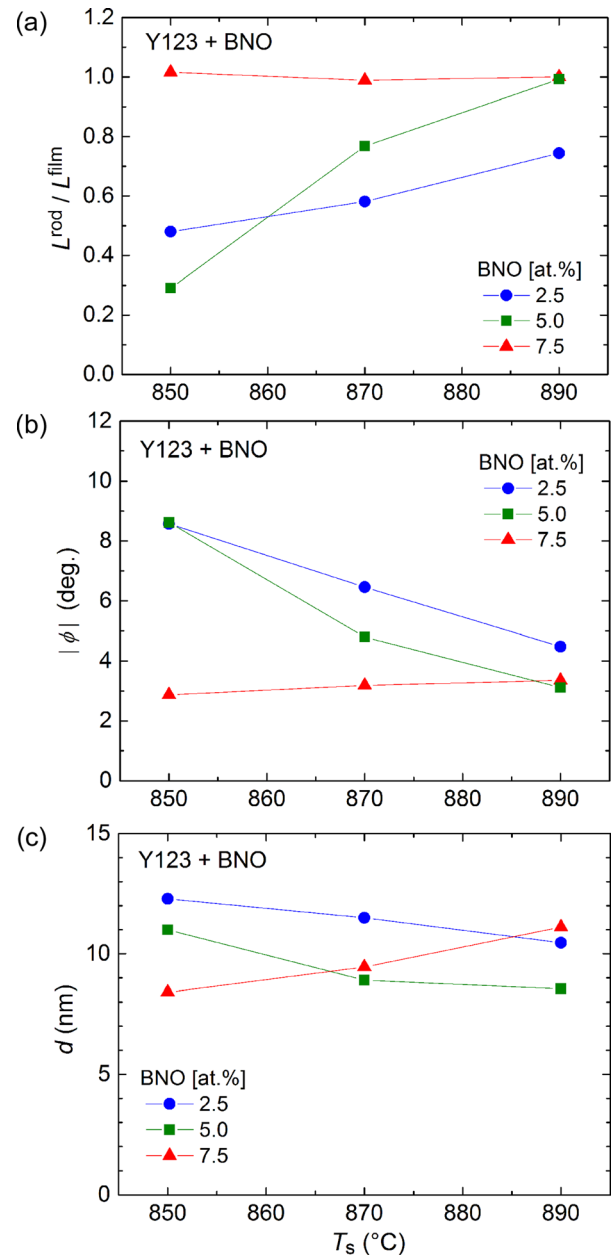
for both films was almost constant. Therefore, one can recognize that the lattice strain along the c-axis was generated in the Y123 matrix by the doping of the BNO nanorod. This is qualitatively consistent with the results in the Y123 films with BZO nanorods.[26,31]

DISCUSSION

As described in Table I, the T_c values for the BNO-doped Y123 films were found to depend on T_s and x. Taking into account that T_c of the RE123 matrix is correlated with the interfacial area of matrix/nanorod for the RE123 films with nanorods,[32] the change in T_c that is dependent on growth conditions suggests that the mean valences of Cu ions in the CuO$_2$ plane of the RE123 matrix were sensitive to the morphology and/or density of the introduced nanorods
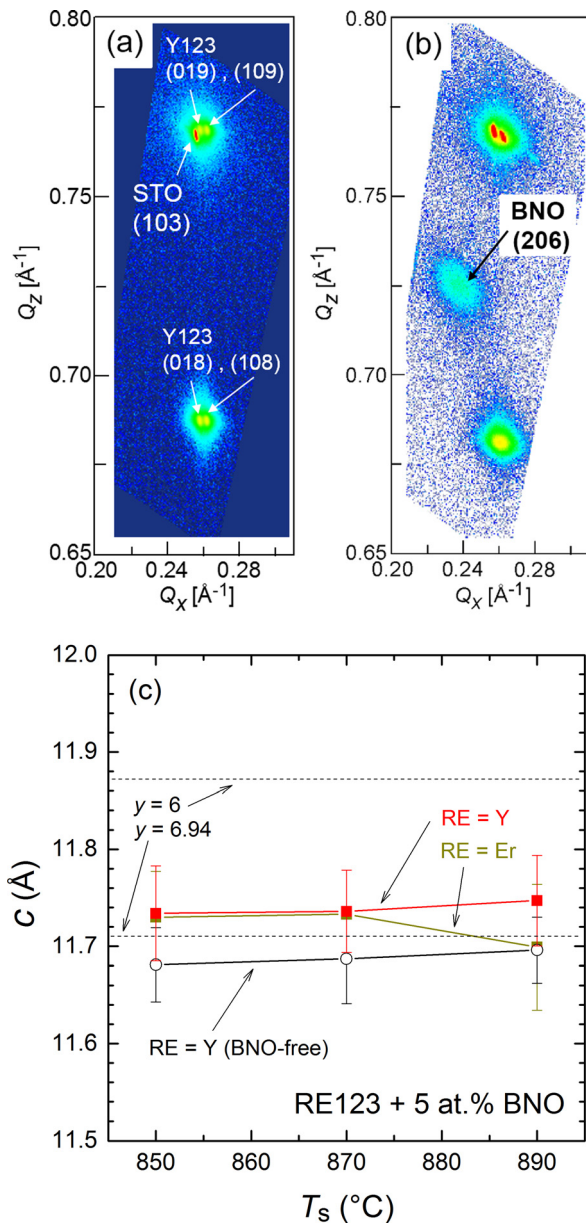
FIG. 4. RSM measurements for (a) BNO-free Y123 films and (b) the BNO-doped ($x = 5$ at. %, $T_s = 890\,°C$) Y123 film; (c) T_s dependence of the $c/3$ values for BNO-free and BNO-doped ($x = 5$ at. %) Y123 films.

and the growth conditions. Additionally, in the present study, T_s- and x-dependent T_cs for the BNO-doped Y123 films suggest that the mean valence of Cu ions is largely affected by T_s and x.

According to a scanning TEM (STEM) analysis with electron energy loss spectroscopy (EELS) for a Y123 film with BZO nanorods by Cantoni *et al.*,[26] all of the strained Y123 regions surrounding the nanorods were oxygen deficient. That is, the carrier-doping levels apparently shift toward an underdoping state with an increase in the densities of the BNO nanorod. Therefore, it is recognized that the reduction in the mean valences of Cu ions due to the reduction of T_c for the BNO-doped Y123 films originates from the expansion of the c-axis length, which was induced by the lattice strain of the matrix through the introduction of BNO nanorods from the above results and the RSM measurements in Fig. 4.

To understand the variation in superconducting properties in the Y123 matrix induced by the interfacial area of the nanorod/matrix for the Y123 films with nanorods, the changes in T_c and B_{irr} at $t = 0.9$ as a function of B_{cr} are shown in Figs. 5(a) and 5(b), respectively. B_{cr} is strongly correlated with the nanorod density, as described in Fig. 1; therefore, B_{cr} is an appropriate experimental parameter for nanorod density. The T_c and B_{irr} values for the BNO-free Y123 film ($T_s = 870\,°C$) are also shown for reference at $B_{cr} = 0$. It should be noted that B_{irr} at $t = 0.9$ was estimated by extrapolation or interpolation using each IL, and only the data for the samples containing and being deduced to contain almost linear morphologies of BNO nanorods with $|\phi| < 5°$ [see Fig. 3(b)] are shown in Fig. 5. As shown in Fig. 5(a), T_c systematically decreased with an increase in B_{cr}. Therefore, T_c and the valence of Cu ions in the CuO$_2$ plane of the Y123 matrix at the matrix/nanorod interface are largely affected by the nanorod densities. However, as shown in Fig. 5(b), B_{irr} at $t = 0.9$ increased with the increase in B_{cr} up to $B_{cr} \sim 5\,T$ and saturated (or decreased) for $B_{cr} > 5\,T$. Masui *et al.*[33] reported that B_{irr} for $B//c$ at $t = 0.9$ in a Y123 single crystal monotonically decreased with the promotion of the underdoping of carriers (or with an increase in oxygen deficiency). In detail, it was reported that the B_{irr} values were drastically changed from $\sim 5\,T$ ($y = 6.96$) to $\sim 1.3\,T$ ($y = 6.77$) despite the samples with $T_c > 90\,K$. Therefore, depletion of the carriers from the optimally carrier-doped level in Y123 seriously decreases the elemental vortex-pinning force. This is quite a contrast to the result for the BNO-doped Y123 films, as seen in Fig. 5(b), strongly indicating that the introduction of nanorods remarkably improved vortex-pinning properties in spite of the T_c reduction induced by the increase in BNO nanorods. Therefore, $B_{cr} \sim 5\,T$ is a boundary field at which the positive vortex-pinning effect due to the nanorods as

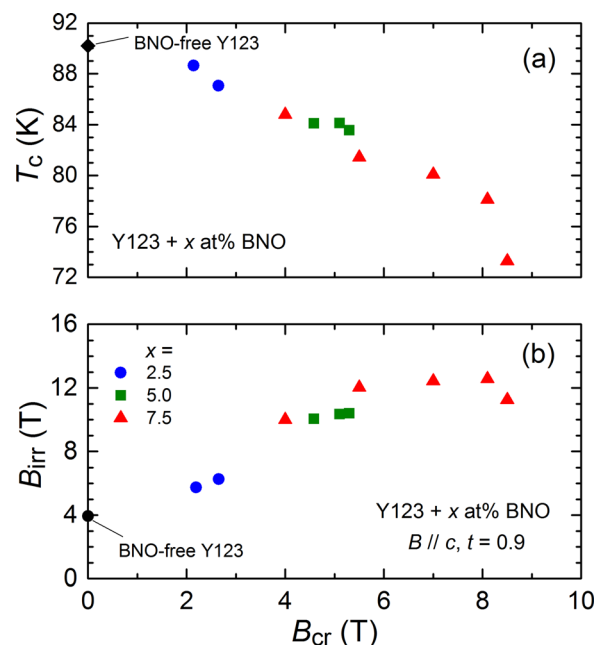FIG. 5. B_{cr} dependences of (a) T_c and (b) B_{irr} at $t = 0.9$ for BNO-doped Y123 films with $x = 0$, 2.5, 5.0, and 7.5 at. %, together with data of a BNO-free Y123 film ($T_s = 870\,°C$).

artificial vortex-pinning centers was suppressed by enhancement of the negative effect due to the T_c reduction of the Y123 matrix.

On the basis of the above discussion in this section, one can quantitatively estimate in the matrix an underdoped Y123 region with a lower T_c, induced by the distortion at the interface, as a distance from the interface (// substrate surface) using the results in Fig. 5. Figure 6 shows a schematic cross-sectional microstructure of the Y123 matrix containing BNO nanorods to assist in understanding the above lattice-strain model. Here, d, l, and D are, respectively, average diameter of the BNO nanorods, distance from the matrix/nanorod interface on a relatively lower T_c region, and average inter-nanorod distance. This model suggests that relatively higher vortex-pinning properties are expected for $D > 2l + d$, whereas a serious reduction of vortex pinning is apparent for $D \leq 2l + d$. Based on the relationship between B_{irr} and y in the Y123 single crystal,[33] the decrease in T_c leads directly to the reduction of B_{irr}. It is well recognized that the B_{irr} value is correlated with the magnitude of vortex-pinning energy through the change in electromagnetic anisotropy[34,35] in high-T_c cuprate superconductors. Additionally, in the case of Y123, a lower T_c region roughly possesses lower vortex-pinning properties. It is likely that all regions of the Y123 matrix are completely dominated by the lower T_c region, which is induced by the lattice strain at the nanorod/matrix interface, at the characteristic B_{cr} value ($\sim 5\,T$) determined in Fig. 5(b). In this case, the inter-vortex distance (D_{vortex}) is calculated to be $\sim 22\,nm$ using the following equation: $B_{cr}/\phi_0 = 2/(\sqrt{3} \times D_{vortex})$.[2] Here, ϕ_0 is a quantized flux. According to the results in Er123+BNO[5,6] and Sm123+BZO,[36] nanorod densities calculated from B_{cr}s (or K_{end} in Ref. 33) in ILs were coincident well with the B_ϕs estimated from microstructures of the nanorods by TEM. This means that appropriate B_{cr}s in RE123 films with nanorods are different from those for the irradiated Y123 crystals,[25,28] in which B_{cr} appeared at $B_\phi/3$.

Taking into account that the nanorod density equals the vortex density determined from B_{cr}, as mentioned above, it is strongly suggested that the inter-nanorod distance (D) coincides with the inter-vortex distance determined from the value of $B_{cr} \sim 5\,T$ ($D_{vortex} \sim 22\,nm$). That is, $D \sim 22\,nm$ can be obtained. From a cross-sectional TEM image for the BNO-doped Y123 thin film ($x = 7.5$ at. %, $T_s = 870\,°C$) with
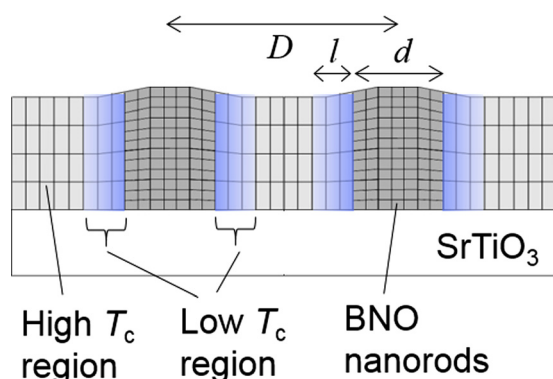

FIG. 6. Schematic model of the cross-sectional microstructure in a Y123 film with BNO nanorods.

$B_{cr} \sim 5.5\,T$ in Fig. 5(b), one can obtain $d \sim 10\,nm$ as average diameter of the BNO nanorods [see Fig. 3(c)]. Therefore, using the above D and d values, $l = 6$–$7\,nm$ can be calculated as an average distance of the lower vortex-pinning region from the interface. As mentioned above, from STEM with EELS for a Y123 film with BZO nanorods, it was found that all of the strained Y123 regions surrounding the nanorods exhibited a lower mean valence of Cu ions and oxygen deficiency and were formed at a distance of $\sim 10\,nm$ from the interface.[17] In this sense, the lower T_c region focused on in the present work almost corresponds with the strained Y123 regions defined in the report by Cantoni *et al.*,[26] and the l value (6–7 nm) estimated from the B_{irr}–B_{cr} curve in Fig. 5(b) roughly coincides with that determined from STEM-EELS for a Y123+BZO film. One can recognize that strained Y123 regions with relatively lower critical current properties can be estimated as the distance from the matrix/nanorod interface using the B_{irr}–B_{cr} curve. This probably means that a maximum value of the density of the BNO nanorods (or B_{cr}) for maximizing B_{irr} for $B//c$ can be precisely determined in principle by determining the mean diameter of the nanorods (d) by microstructural analysis. Choosing nanorod materials with smaller diameters and a shorter l is one of material-scientific strategies for further improving B_{irr} in Y123 films with nanorods.

CONCLUSION

In conclusion, the present study clarified the x and T_s dependences of critical current properties, microstructures of BNO nanorods, and c-axis lengths of the Y123 matrix for Y123+BNO films with a different x and T_s. The values of B_{irr} at $t = 0.9$ and B_{cr}, which were determined from the vortex-Bose-glass-like ILs, were largely dependent on both x and T_s. Consequently, B_{irr} exhibited a maximum value at $B_{cr} \sim 5\,T$ in spite of the monotonic reduction in T_c with an increase in B_{cr}. This indicates that the respective effects of enhancement and deterioration of vortex-pinning properties due to the increase in c-axis-correlated pinning centers and the T_c reduction of the strained Y123 region by the introduction of nanorods are competitive in the Y123+BNO films, and the deterioration effect by the strained Y123 region is dominant for $B_{cr} > 5\,T$. Consequently, in the case of the Y123+BNO film, $l = 6$–$7\,nm$ was obtained. Our present study indicates that control of the strained region and/or l is important for enhancing the maximum value of B_{irr} in RE123 films with nanorods.

[1]J. L. Macmanus-Driscoll, S. R. Foltyn, Q. X. Jia, H. Wang, A. Serquis, B. Maiorov, L. Civale, M. E. Hawley, M. P. Maley, and D. E. Peterson, Nat. Mater. **3**, 439 (2004).

[2]S. A. Harrington, J. H. Durrell, B. Maiorov, H. Wang, S. C. Wimbush, A. Kursumovic, J. H. Lee, and J. L. MacManus-Driscoll, Supercond. Sci. Technol. **22**, 022001 (2009).

[3]P. Mele, K. Matsumoto, T. Horide, A. Ichinose, M. Mukaida, Y. Yoshida, S. Horii, and R. Kita, Supercond. Sci. Technol. **21**, 032002 (2008).

[4]M. Peurla, P. Paturi, Y. P. Stepanov, H. Huhtinen, Y. Y. Tse, A. C. Bòdi, J. Raittila, and R. Laiho, Supercond. Sci. Technol. **19**, 767 (2006).

[5]S. Horii, K. Yamada, H. Kai, A. Ichinose, M. Mukaida, R. Teranishi, R. Kita, K. Matsumoto, Y. Yoshida, J. Shimoyama, and K. Kishio, Supercond. Sci. Technol. **20**, 1115 (2007).

[6]S. Horii, H. Kai, M. Mukaida, K. Yamada, R. Teranishi, A. Ichinose, K. Matsumoto, Y. Yoshida, R. Kita, J. Shimoyama, and K. Kshio, Appl. Phys. Lett. **93**, 152506 (2008).

[7]G. Ercolano, M. Bianchetti, S. C. Wimbush, S. A. Harrington, H. Wang, J. H. Lee, and J. L. MacManus-Driscoll, Supercond. Sci. Technol. **24**, 095012 (2011).

[8]T. Horide, T. Kawamura, K. Matsumoto, A. Ichinose, M. Yoshizumi, T. Izumi, and Y. Shiohara, Supercond. Sci. Technol. **26**, 075019 (2013).

[9]M. Mukaida, T. Horide, R. Kita, S. Horii, A. Ichinose, Y. Yoshida, O. Miura, K. Matsumoto, K. Yamada, and N. Mori, Jpn. J. Appl. Phys., Part 2 **44**, L952 (2005).

[10]Y. Yamada, K. Takahashi, H. Kobayashi, M. Konishi, T. Watanabe, A. Ibi, T. Muroga, S. Miyata, T. Kato, T. Hirayama, and Y. Shiohara, Appl. Phys. Lett. **87**, 132502 (2005).

[11]S. Kang, A. Goyal, J. Li, A. A. Gapud, P. M. Martin, L. Heatherly, J. R. Thompson, D. K. Christen, F. A. List, M. Paranthaman, and D. F. Lee, Science **311**, 1911 (2006).

[12]B. Maiorov, S. A. Baily, H. Zhou, O. Ugurlu, J. A. Kennison, P. C. Dowden, T. G. Holesinger, S. R. Foltyn, and L. Civale, Nat. Mater. **8**, 398 (2009).

[13]F. J. Baca, T. J. Haugan, P. N. Barnes, T. G. Holesinger, B. Maiorov, R. Lu, X. Wang, J. N. Reichart, and J. Z. Wu, Adv. Funct. Mater. **23**, 4826 (2013).

[14]V. Selvamanickam, Y. Chen, T. Shi, Y. Liu, N. D. Khatri, J. Liu, Y. Yao, X. Xiong, C. Lei, S. Soloveichik, E. Galstyan, and G. Majkic, Supercond. Sci. Technol. **26**, 035006 (2013).

[15]K. Yamada, M. Mukaida, H. Kai, R. Teranishi, A. Ichinose, R. Kita, S. Kato, S. Horii, Y. Yoshida, K. Matsumoto, and S. Toh, Appl. Phys. Lett. **92**, 112503 (2008).

[16]G. Ercolano, S. A. Harrington, H. Wang, C. F. Tsai, and J. L. MacManus-Driscoll, Supercond. Sci. Technol. **23**, 022003 (2010).

[17]D. M. Feldmann, T. G. Holesinger, B. Maiorov, S. R. Foltyn, J. Y. Coulter, and I. Apodaca, Supercond. Sci. Technol. **23**, 095004 (2010).

[18]S. H. Wee, A. Goyal, Y. L. Zuev, C. Cantoni, V. Selvamanickam, and E. D. Specht, Appl. Phys. Exp. **3**, 023101 (2010).

[19]S. H. Wee, A. Goyal, E. D. Specht, C. Cantoni, Y. L. Zuev, V. Selvamanickam, and S. Cook, Phys. Rev. B **81**, 140503(R) (2010).

[20]Y. Shingai, T. Numasawa, M. Mukaida, R. Teranishi, R. Kita, A. Ichinose, S. Horii, Y. Yoshida, K. Matsumoto, S. Awaji, K. Watanabe, A. Saito, K. Yamada, and N. Mori, Physica C **463**, 909 (2007).

[21]H. Tobita, K. Notoh, K. Higashikawa, M. Inoue, T. Kiss, T. Kato, T. Hirayama, M. Yoshizumi, T. Izumi, and Y. Shiohara, Supercond. Sci. Technol. **25**, 062002 (2012).

[22]A. Xu, L. Delgado, N. Khatri, Y. Liu, V. Selvamanickam, D. Abraimov, J. Jaroszynski, F. Kametani, and D. C. Larbalestier, APL Mater. **2**, 046111 (2014).

[23]S. Awaji, Y. Yoshida, T. Suzuki, K. Watanabe, K. Hikawa, Y. Ichino, and T. Izumi, Appl. Phys. Exp. **8**, 023101 (2015).

[24]M. Haruta, A. Ichinose, N. Fujita, Y. Ogura, T. Nakata, T. Maeda, and S. Horii, Appl. Phys. Express **5**, 073102 (2012).

[25]L. Krusin-Elbaum, L. Civale, G. Blatter, A. D. Marwick, F. Holtzberg, and C. Feild, Phys. Rev. Lett. **72**, 1914 (1994).

[26]C. Cantoni, Y. Gao, S. H. Wee, E. D. Specht, J. Gazquez, J. Meng, S. J. Pennycook, and A. Goyal, ACS Nano **5**, 4783 (2011).

[27]A. Ichinose, K. Naoe, T. Horide, K. Matsumoto, R. Kita, M. Mukaida, Y. Yoshida, and S. Horii, Supercond. Sci. Technol. **20**, 1144 (2007).

[28]L. Civale, A. D. Marwick, T. K. Worthington, M. A. Kirk, J. R. Thompson, L. Krusin-Elbaum, Y. Sun, J. R. Clem, and F. Holtzberg, Phys. Rev. Lett. **67**, 648 (1991).

[29]A. Mazilu, H. Safar, M. P. Maley, J. Y. Coulter, L. N. Bulaevskii, and S. Foltyn, Phys. Rev. B **58**, R8909 (1998).

[30]J. Ye and K. Nakamura, Phys. Rev. B **48**, 7554 (1993).

[31]T. Horide, T. Kitamura, A. Ichinose, and K. Matsumoto, Jpn. J. Appl. Phys., Part 1 **53**, 083101 (2014).

[32]M. Namba, S. Awaji, K. Watanabe, S. Ito, E. Aoyagi, H. Kai, M. Mukaida, and R. Kita, Appl. Phys. Express **2**, 073001 (2009).

[33]T. Masui, Y. Takano, K. Yoshida, K. Kajita, and S. Tajima, Physica C **412–414**, 515 (2004).

[34]J. Shimoyama, K. Kitazawa, K. Shimizu, S. Ueda, S. Horii, N. Chikumoto, and K. Kishio, J. Low Temp. Phys. **131**, 1043 (2003).

[35]K. Takenaka, K. Mizuhashi, H. Takagi, and S. Uchida, Phys. Rev. B **50**, 6534 (1994).

[36]T. Ozaki, Y. Yoshida, Y. Ichino, Y. Takai, A. Ichinose, K. Matsumoto, S. Horii, M. Mukaida, and Y. Takano, J. Appl. Phys. **108**, 093905 (2010).